THE ASTROPHYSICAL JOURNAL, 444:561–566, 1995 May 10

TIME DELAY IN THE EINSTEIN RING PKS 1830−211

T. D. VAN OMMEN,[1] D. L. JONES, AND R. A. PRESTON
Jet Propulsion Laboratory, California Institute of Technology

AND

D. L. JAUNCEY
Australia Telescope National Facility, P.O. Box 76, Epping, NSW 2121, Australia
Received 1994 September 14; accepted 1994 November 16

ABSTRACT

We present radio observations of the gravitational lens PKS 1830−211 at 8.4 and 15 GHz acquired using the Very Large Array. The observations were made over a 13 month period. Significant flux density changes over this period provide strong constraints on the time delay between the two lensed images and suggest a value of 44 ± 9 days. This offers new direct evidence that this source is indeed a gravitational lens. The lens distance is dependent upon the model chosen, but reasonable limits on the mass of the lensing galaxy suggest that it is unlikely to be at a redshift less than a few tenths, and may well be significantly more distant.

Subject headings: galaxies: individual (PKS 1830−211) — gravitational lensing — radio continuum: galaxies

1. INTRODUCTION

The highly symmetrical double structure of the flat-spectrum radio source PKS 1830−211 was first identified by Rao & Subrahmanan (1988) who suggested that this unusual combination of properties may be the result of gravitational lensing of a single flat-spectrum source. Further observations (Jauncey et al. 1991) show a low-level ring of emission linking the two components in a manner consistent with an Einstein ring—a configuration in which the lensing mass is very closely aligned with a part of the lensed object.

This source is by far the brightest radio source of any gravitational lens candidate (flux density ≈ 10 Jy at 2.3 GHz) and is highly variable (in a recent outburst, the 8.4 GHz flux density doubled). These properties make PKS 1830−211 an attractive candidate for monitoring of the individual component flux densities, with the ultimate aim of determining the differential time delay between the two images. So far, attempts to optically identify the lensing object have proved unsuccessful (Jauncey et al. 1991; Djorgovski et al. 1992; Jauncey et al. 1993), but should such an identification (and redshift measurement) be made, a time delay measurement would enable modeling of the system to provide an estimate of Hubble's constant (Refsdal 1964) at high redshift.

The observations described here were undertaken to investigate the flux density variability between the two components. A short series of monthly snapshots and a later series of daily snapshots were taken using the Very Large Array (VLA)[2] over a 13 month period in 1990–1991. These reveal relative flux density variations between the two components during this time. Intensive single dish measurements of total flux density (Jauncey et al. 1993) made over this period show dramatic flux density variations, providing a means of estimating the delay from the otherwise undersampled series of VLA images.

2. OBSERVATIONS AND DATA ANALYSIS

2.1. *Observations*

A series of observations using the VLA were made in sessions from 1990 June through 1991 July. The observations were made in the A, BnA,[3] and B configurations at frequencies of 8.4 and 15 GHz. The 15 GHz data were primarily intended to provide useful resolution while the VLA was in more compact configurations.

All observations were made with a total bandwidth of 100 MHz, split into two adjacent 50 MHz bands and correlated for both senses of circular polarization. Table 1 details the configuration, frequency, beam parameters, and effective integration time for each of the imaged data sets. The center-frequencies for the bands were the standard VLA values of 8415/8465 and 14915/14965 MHz for the "8.4" and "15" GHz bands, respectively.

2.2. *Calibration and Imaging*

With two exceptions, the flux density measurements reported here are referred to the radio source 3C 286. The exceptions are the 1991 July 6 data, which are referred to 3C 48 and the observation of 1990 September 18, for which absolute flux density calibration was not possible as no appropriate calibrator was observed. The flux densities are based on the scale of Baars et al. (1977) and are applied to the data in the conventional manner using the Astronomical Image Processing System (AIPS) package.

Short observations of nearby VLA phase calibrator sources were made once or twice in each observing session and used to compute antenna gains. The sources used were J1832−105 for the 1990 sessions and J1911−201 for the 1991 sessions. We used the VLA Calibrator List positions (J2000) for these sources:[4] $\alpha = 18^h32^m20^s.8437$, $\delta = -10°35'11''.300$; $\alpha = 19^h11^m09^s.6530$, $\delta = -20°06'55''.109$. The uncertainties quoted for these positions are greater than 15 milliarcsec (mas) and less

[1] Now at Antarctic CRC, University of Tasmania, GPO Box 252C, Hobart, TAS, 7001, Australia.

[2] The Very Large Array is a facility of the National Radio Astronomy Observatory, which is operated by Associated Universities, Inc., under contract with the National Science Foundation.

[3] The BnA configuration is suited to observations of sources south of declinations of about −15°. In this mode the array is nominally in its B configuration, with the North arm antennas deployed as for the A configuration.

[4] We use the convention here that α denotes right ascension coordinates and δ denotes declination.

TABLE 1

OBSERVING PARAMETERS FOR IMAGED DATA SETS

DATE	DOY (1990)	FREQUENCY (GHz)	EQUIVALENT INTEGRATION TIME[a]	VLA CONFIGURATION	BEAM[b]		
					Major Axis	Minor Axis	P.A.
1990 Jun 11	162	8.4	10^{m}45^s	BnA	0.″37	0.″27	−22.°4
1990 Jul 6	187	8.4	39 07	BnA	0.60	0.38	−87.6
		15	78 23	BnA	0.26	0.19	84.5
1990 Aug 16.....	228	8.4	15 28	B	1.00	0.59	14.4
1990 Sep 18	261	8.4	3 28	B	1.16	0.66	2.7
		15	10 00	B	0.59	0.34	−2.6
1991 Jul 2	548	8.4	5 15	A	0.26	0.19	26.6
		15	9 15	A	0.16	0.11	24.3
1991 Jul 5	551	8.4	10 34	A	0.32	0.17	7.3
1991 Jul 6	552	8.4	6 56	A	0.24	0.19	30.3
1991 Jul 7	553	8.4	4 31	A	0.24	0.19	29.6
		15	7 14	A	0.15	0.11	27.1
1991 Jul 8	554	8.4	6 21	A	0.34	0.20	−1.0
1991 Jul 12	558	8.4	6 25	A	0.28	0.18	−20.7
1991 Jul 13	559	8.4	6 59	A	0.32	0.18	12.2
		15	9 16	A	0.18	0.10	9.9
1991 Jul 17	563	8.4	5 19	A	0.34	0.19	−0.6
		15	9 57	A	0.19	0.10	−1.4

[a] Computed as equivalent time with all 27 antennas.
[b] FWHM of the major and minor axes of the synthesized beam, and the position angle measured north to east.

than 2 mas, respectively. We used the AIPS package to calibrate and map the data. The data were deconvolved using the CLEAN algorithm (AIPS task MX) and self-calibrated with the task CALIB. Self-calibration was typically ahieved in several passes, using a limited number of the clean components from each deconvolution as the input model for subsequent passes. Early self-calibration iterations were limited to phase-only calibration, before full amplitude self-calibration was allowed in the final stages. Gain normalization was used in the amplitude self-calibration passes to retain absolute flux density calibration.

3. RESULTS

3.1. *Images*

Figures 1 and 2 show images taken at 8.4 GHz (1991 July 7) and 15 GHz (1991 July 17), respectively. These images illustrate the features seen in the other data sets and are representative of the higher quality images made. The images from the several sessions vary in appearance and quality, due to the vagaries of weather and the beam-shape, which in turn depends on the array configuration and the hour-angle of the observation. The images do show variations in the relative strength of the two bright components which are discussed in the next section.

Most of the 15 GHz images show a weak (≈0.5%–1.0% SW component peak) low-level feature at around 0.″3 NE of the SW component. Other workers (Subrahmanyan et al. 1990, hereafter SNRS; Nair, Narasimhar, & Rao 1993, hereafter NNR) have suggested that this may be a "third image" of the background source.

The positions of the two main components have been computed fom the 8.4 GHz observation of 1991 July 2 (and so are referred to the position of J1911−201 given in the previous section). These positions are $\alpha = 18^h33^m39^s.94$, $\delta = -21°03'39''.7$ and $\alpha = 18^h33^m39^s.89$, $\delta = -21°03'40''.4$ with an estimated accuracy of approximately 0.1 arcsecond (Perley 1994).

3.2. *Variability and Limits on the Lensing Delay*

Figure 3 shows the flux density values measured from these VLA observations together with a section of data from a single dish flux density monitoring survey being conducted at the University of Tasmania (Jauncey et al. 1993). The individual component flux densities have been derived by fitting Gaussians to the two components and using the total integrated intensities. In this way, the values are insensitive to the changes in beam orientation and size throughout the observing period.

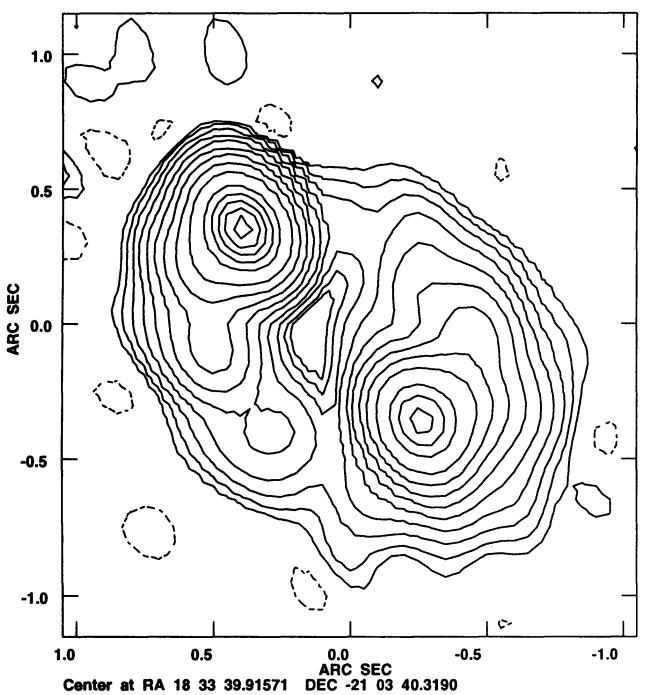

FIG. 1.—8.4 GHz image from 1991 July 7. Contours are at −0.05, 0.05, 0.1, 0.2, 0.4, 0.8, 1.6, 3.2, 6.4, 12.8, 30.0, 45.0, 60.0, 75.0, and 90.0 percent of the peak flux density (2.861 Jy beam^{-1}).

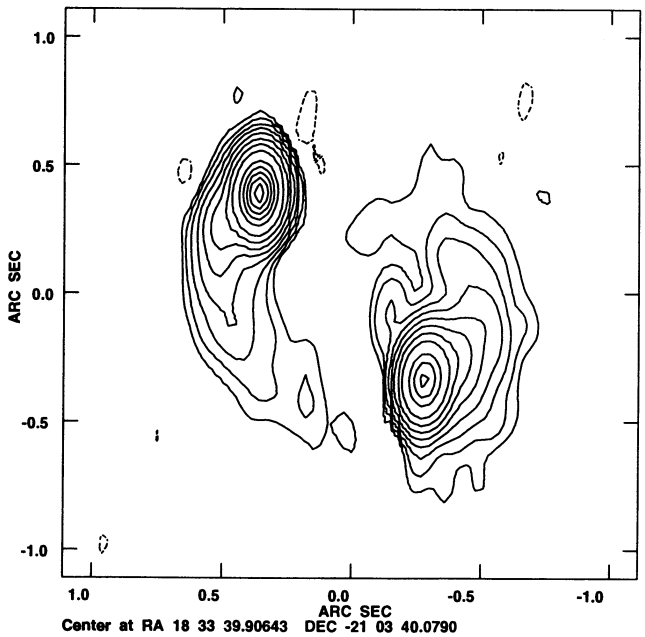

FIG. 2.—15 GHz image from 1991 July 17. Contours are at −0.1, 0.1, 0.2, 0.4, 0.8, 1.6, 3.2, 6.4, 12.8, 30.0, 45.0, 60.0, 75.0, and 90.0 percent of the peak flux density (3.405 Jy beam^{-1}).

The total and component flux densities are relatively constant during the observations in 1990 (days 162 to 228), and both total flux density and flux density in the NE component have increased by the 1991 epoch (near day 555 on the graph). These data are tabulated in Table 2, together with the ratio of component flux densities in the sense NE/SW flux density. This ratio shows a remarkable constancy during the monthly series of observations in 1990 and again within the daily observations in 1991. The flux density values for the observation of day 261 do not appear in Figure 3 because there is no absolute flux density calibration for this epoch. Nevertheless, it is worth noting the the flux density ratio is very similar to the earlier epochs.

Figure 4 shows the 15 GHz flux density measurements. Clearly, in contrast to the 8.4 GHz data, we no longer have the benefit of a well-sampled series of total flux density measurements and so we cannot characterize the shape of the light curve between the 1990 and 1991 observations. Also, absolute calibration of the 15 GHz data is a more serious problem than at 8.4 GHz. Nevertheless, we see from the tabulated values in Table 3 that the ratios are again highly reproducible.

These data may be used to place limits on the lensing time delay by considering how flux density changes with a delay lead to changes in the component flux density ratio. Clearly, if the imaged background object brightens on a timescale comparable with the lensing delay then one image (component) will brighten ahead of the other and the observed flux density ratio will change. In fact, this appears to be the situation seen here. The flux density ratio (NE/SW) measured in the 1991 observations, while the overall flux density is increasing, is considerably larger than the ratio measured in 1990 when flux density was nearly constant. This is consistent with the interpretation that the SW image is delayed with respect to the NE image, and indeed this is the sense of delay indicated by gravitational lens models of this source (SNRS, NNR).

Before we can seek a quantitative relationship between the observed changes in flux density and component ratio and the time delay, we must address the fact that this source is not

TABLE 2

1830−211 8.4 GHz FLUX DENSITIES FROM VLA IMAGES

Day of Year (1990)	Total Flux Density (Jy)	NE Component (Jy)	SW Component (Jy)	Ratio R
162.....	5.01	2.57	2.20	1.17
187.....	5.25	2.71	2.34	1.16
228.....	5.26	2.77	2.37	1.17
261.....	...	...	...	1.15
548.....	6.29	3.18	2.39	1.33
551.....	5.2	2.98	2.28	1.31
552.....	5.71	2.88	2.17	1.33
553.....	6.35	3.20	2.42	1.32
554.....	5.84	3.04	2.33	1.30
558.....	5.77	3.01	2.26	1.33
559.....	6.15	3.15	2.40	1.31
563.....	6.13	3.18	2.43	1.31

NOTES.—Total flux densities are totals cleaned from the image. Component flux densities are integrated over gaussians fitted to each component above the 10% level.

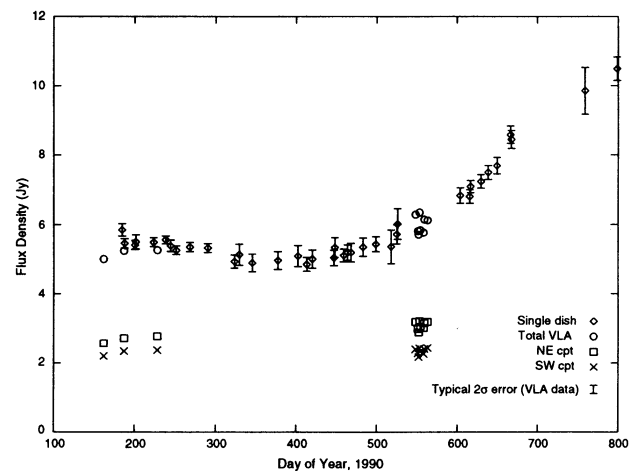

FIG. 3.—1830−211 8.4 GHz flux densities, 1990–1991. Error bars indicate a ±1 σ interval. The abscissa is scaled in units of days, commencing wth 1 on 1990 January 1.

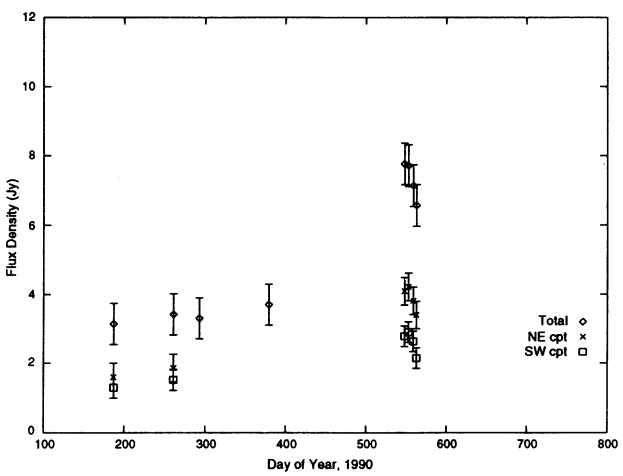

FIG. 4.—1830−211 15 GHz flux densities, 1990–1991

TABLE 3

1830−211 15 GHz Flux Densities from VLA Images

Day of Year (1990)	Total Flux Density (Jy)	NE Component (Jy)	SW Component (Jy)	Ratio R
187.....	3.14	1.59	1.29	1.23
261.....	3.42	1.85	1.51	1.23
293.....	3.3	...	...	
379.....	3.7	...	...	
548.....	7.76	4.09	2.78	1.47
553.....	7.71	4.22	2.90	1.46
559.....	7.14	3.81	2.63	1.45
563.....	6.57	3.40	2.14	1.45

Notes.—Total flux densities are totals cleaned from the image. Component flux densities are integrated over Gaussians fitted to each component above the 10% level.

believed to consist of two simple images of a point source. There are other components to this image which may be contributing to the observed changes.

Current understanding of this source (SNRS, NNR) suggests that it is an image of a background object comprising three distinct components: A relatively flat spectrum core, a steeper spectrum jet, and a knot within the jet. It is the jet which most nearly aligns with the lensing mass and produces the ring emission, particularly at lower frequencies. The core is imaged in the two dominant components on the NE and SW of the ring. The images of the knot are very close to those of the core ($\approx$0.1–0.2 arcsec) and are only distinguishable from the core in VLA maps at 15 GHz and above (SNRS).

Variability in 1830−211 is almost certainly confined to the core component. VLBI studies (King 1994) show that the increase in brightness seen in Figure 3 is confined to the compact components. Also, comparison between the single dish flux densities and the combined flux density of the NE and SW components suggests little or no variation in the ring flux density. (Note that it is misleading to use the total cleaned flux density from the images as tabulated in Table 2 as this varies with the quality of the data and consequently the depth to which the image was cleaned. In particular, the monthly data from 1990 are of lower quality and give totals which are missing some of the ring flux density.)

It is apparent then that due to the close proximity of the knot and core images the measured NE to SW component ratio is a combination of the actual lens magnifications for these two objects. This effect will be less pronounced at higher frequencies where the relative weakening of the steeper spectrum knot (and improved resolution) produce ratios which are dominated by the core. It follows that because of spectral differences, the observed ratio will be frequency dependent, and indeed this appears to be the case. The results at 8.4 and 15 GHz detailed here, and a more extensive tabulation of data from 1.49 to 22.5 GHz (NNR) suggest a generally increasing trend in ratio with increasing frequency. Comparisons of ratios from different epochs are, however, confounded by the effect of variability on the same timescale as the lens delay.

Turning to the observations presented here, we note from Table 2 that the measured ratios and flux densities at 8.4 GHz show little or no change over a 100 day period, and similarly at 15 GHz (Table 3) there is a period of 75 days in which the ratio and flux density is approximately constant. We know, however, that for a 1 arcsecond image separation, reasonable limits on the mass and redshift of the lensing galaxy lead to estimates of the order of days to several tens of days for the time delay (SNRS; Jauncey et al. 1993; NNR). So the ratios measured during this quiescent period will be unaffected by time delay effects. Consequently the different quiescent ratios (1.17 and 1.23 at 8.4 GHz and 15 GHz, respectively) are reflective of an underlying frequency dependence and not merely the result of variability.

We now turn our attention to quantitative relationships between the various observables. We begin by constructing a two-component model for the compact components, writing

$$F_{\rm SW}(t) = C_{\rm SW}(t) + K_{\rm SW} , \tag{1}$$

where $F_{\rm SW}(t)$ is the flux density of the SW component, $C_{\rm SW}(t)$ is the flux density of the core and $K_{\rm SW}$ is the (constant) flux density of the SW knot. We also define $F_{\rm NE}(t)$, $C_{\rm NE}(t)$, and $K_{\rm NE}$ analogously for the NE component. Then, if the time delay between the two images is Δt and R_c is the ratio of magnifications for the two images of the core:

$$R_c = \frac{C_{\rm NE}(t - \Delta t)}{C_{\rm SW}(t)} , \tag{2}$$

which is, of course, time and frequency independent. Similarly, if R_k is the ratio of magnifications for the two knot images,

$$R_k = \frac{K_{\rm NE}}{K_{\rm SW}} .$$

It is useful to recast equation (2) as follows:

$$C_{\rm NE}(t) = R_c\, C_{\rm SW}(t + \Delta t) .$$

The NE component flux density can then be written entirely in terms of the SW knot and core:

$$F_{\rm NE}(t) = RcC_{\rm SW}(t + \Delta t) + R_k K_{\rm SW} .$$

So the observed flux density ratio, $R(t)$ can be written

$$R(t) = \frac{F_{\rm NE}(t)}{F_{\rm SW}(t)} = \frac{R_c\, C_{\rm SW}(t + \Delta t) + R_k K_{\rm SW}}{C_{\rm SW}(t) + K_{\rm SW}} . \tag{3}$$

Next we use a first-order expansion of $C_{\rm SW}(t)$ to approximate $C_{\rm SW}(t + \Delta t)$,

$$C_{\rm SW}(t_0 + \Delta t) \approx a + b\,\Delta t ,$$

where $a = C_{\rm SW}(t_0)$ and $b = [dC_{\rm SW}(t_0)]/dt$. Thus, using R as shorthand for $R(t_0)$,

$$R = \frac{R_c(a + b\,\Delta t) + R_k K_{\rm SW}}{a + K_{\rm SW}} ,$$

from which we can obtain

$$\Delta t = \frac{a(R - R_c) + K_{\rm SW}(R - R_k)}{bR_c} . \tag{4}$$

We know that the total flux density of the source, $F(t)$ is the sum of the two compact components and a constant ring flux density, F_R, namely

$$F(t) = F_{\rm NE}(t) + F_{\rm SW}(t) + F_R ,$$

so taking the time derivative and using the notation $F' \equiv [dF(t)]/dt$ we get (with our first-order approximation)

$$F' = F'_{\rm NE} + F'_{\rm SW}$$
$$\approx R_c\, b + b .$$

TABLE 4

INPUT PARAMETERS TO MODEL

Parameter	8.4 GHz	15 GHz
SW knot flux density[a] K_{SW}	...	0.18 ± 0.01
Quiescent SW component flux density F_q	2.30 ± 0.09	1.40 ± 0.33
Quiescent flux density ratio R_q	1.17 ± 0.01	1.23 ± 0.01
Day 555 SW component flux density F_{SW}	2.34 ± 0.09	2.61 ± 0.33
Day 555 flux density ratio R	1.32 ± 0.01	1.46 ± 0.01
Day 555 total flux density slope F'	0.0140 ± 0.0006	0.021 ± 0.005

[a] From SNRS 15 GHz data.

This gives b in terms of F' which can be estimated from the single-dish data:

$$b = \frac{F'}{1 + R_c} . \quad (5)$$

Next, use F_{SW} as shorthand for $F_{SW}(t_0)$. Then, from equation (1) and the linear approximation for C_{SW} we can write

$$a = F_{SW} - K_{SW} . \quad (6)$$

Equations (4), (5), and (6) allow us to write Δt as

$$\Delta t = \frac{[F_{SW}(R - R_c) + K_{SW}(R_c - R_k)](R_c + 1)}{F' R_c} . \quad (7)$$

The three quantities R_c, K_{SW}, and R_k in equation (7) are not immediately available from the data in Tables 2 and 3. We do, however, have additional information in the form of the quiescent ratios (as discussed above), which we denote R_q. Making use of the fact that during quiescent observations flux density is constant, and so, $C_{SW}(t + \Delta t) = C_{SW}(t)$, (which in turn we shall write as C_q) and recalling equation (3) we get

$$R_q = \frac{R_c C_q + R_k K_{SW}}{C_q + K_{SW}} .$$

This then gives R_c:

$$R_c = \frac{R_q F_q - R_k K_{SW}}{F_q - K_{SW}} , \quad (8)$$

where $F_q = C_q + K_{SW}$ is the quiescent SW component flux density.

This leaves us without K_{SW}, the SW knot flux density, and R_k, the knot ratio. SNRS give 15 GHz values for the knot flux densities which solve this problem, at least at this frequency, provided the assumption is made that the knot flux is not time variable. This then provides a value of R_c from the 15 GHz data and because this quantity is not frequency dependent it may be used to estimate K_{SW}, the knot flux density, at 8.4 GHz via equation (8). In practical terms, the knot ratio, R_k is not well constrained by the data of SNRS, and the approach has been taken wherein delays are computed for several different knot ratios.

The actual parameter values used are shown in Table 4. The 15 GHz value of the SW knot flux density is based on the SNRS value as discussed above. The total flux density slope for the 8.4 GHz data is computed from a least-squares fit to the single dish data in the region of day 555. The error is formally computed from the fit and the errors in the individual measurements. The slope in total flux density at 15 GHz is estimated by assuming an approximately linear increase in flux from day 379 to day 555 (Fig. 4). From this we can infer a slope of approximately 16–25 mJy day^{-1}. All other errors in Table 4 are estimated from the scatter in the values themselves.

Table 5 shows the derived values for time delay, core ratio and 8.4 GHz knot flux density for the input parameters of Table 4 and a range of likely knot ratios.

More detailed examination of the model behavior confirms the relative insensitivity of the computed delay to the particular choice of knot ratio, R_k. However, as the knot ratio increases above 0.9, the SW knot flux density, K_{SW} at 8.4 GHz increases sharply to unlikely levels (as required for a consistent core ratio at both frequencies). Thus, we adopt a value of around 0.7 for the likely knot ratio and estimate the time delay as 44 ± 9 days.

Finally, if the knot flux is neglected completely from the analysis, equation (8) gives $R_c = R_q$. This obviously makes it impossible to reconcile the discrepant quiescent ratios observed at 15 and 8.4 GHz, however, it does simplify the analysis, giving an expression for Δt (from eq. [7]):

$$\Delta t = \frac{F_{SW}(R - R_q)(R_q + 1)}{F' R_q} .$$

This gives time delays of 46 ± 5 and 53 ± 13 days for the 8.4 and 15 GHz input parameters—values which do not differ greatly from the more realistic core plus knot model investigated above.

4. CONCLUDING REMARKS

It is clear from these observations that both components of PKS 1830−211 participate in brightness fluctuations in a manner consistent with a delay of around 44 days. This provides new and very strong evidence that this source is indeed a gravitational lens system. The magnitude of the lensing delay is at the upper end of the ranges predicted by attempts to model PKS 1830−211 as a gravitational lens (SNRS; NNR). Unfortunately, modeling attempts are confounded by the lack of an optical identification and hence a redshift for the lensing galaxy. SNRS obtain the following approximate relation for the lensing delay, Δt:

$$\Delta t \sim 6(z_g/0.1)(2h)^{-1} \text{ days} ,$$

TABLE 5

DERIVED PARAMETERS FROM MODEL

	Derived Parameters			
		SW Knot Flux Density at 8.4 GHz (Jy)	Time Delay	
Input Knot Ratio	Core Ratio		8.4 GHz (days)	15 GHz (days)
0.9	1.28 ± 0.02	0.66 ± 0.10	44 ± 7	46 ± 13
0.7	1.31 ± 0.02	0.52 ± 0.08	44 ± 9	43 ± 12
0.5	1.34 ± 0.03	0.46 ± 0.08	43 ± 12	39 ± 12

where h is the Hubble constant in units of 100 km s^{-1} Mpc^{-1} and z_g is the redshift of the lensing galaxy. From this relation, and limits on the mass of the lensing galaxy (which is also a function of redshift) they suggest a delay of 2–20 days. NNR predict a wider range of delays, from days to several tens of days for a reasonable range of redshifts. From their model we find that a delay of 44 days gives masses for the lensing galaxy of 9×10^{11} and 8×10^{11} $M_\odot$ for lens redshifts of 0.3 and 0.5, respectively.

The model of NNR relies quite heavily for its constraints on a small number of tabulated values of R (the flux density ratio between the NE and SW components) at different frequencies and epochs. They explicitly neglect time delay effects on R and conclude that it increases with frequency. The data presented here imply quiescent flux density ratios of 1.17 and 1.23 at 8.4 GHz and 15 GHz, respectively. These values are substantially lower than the values available to NNR and they imply a much more modest increase with frequency. Consequently, these results will affect the predictions of their model.

It is readily apparent from these observations and those of Jauncey et al. (1993) that PKS 1830−211 displays large flux density changes over timescales comparable to the lensing delay. Further, these changes are not seen simultaneously at all frequencies and so lead to dramatic changes in spectral index, as seen here between 8.4 and 15 GHz over a 1 year period. This highlights the necessity of ongoing multifrequency monitoring in order to determine spectra of the individual components and to further refine the time delay measurement.

The suspected "third" image of the source seen in the 15 GHz data is also of considerable interest. Further observations are required to establish the relationship between this feature and the other two images. It is possible that a series of 15 or 22 GHz observations made with sufficient frequency could determine the time delay of this image relative to the others in much the same way as has been done with the two stronger images here. A time delay for this image, or even simply confirmation that it is an image, would help to constrain source models.

Finally, this work provides fresh impetus to optical searches directed at detecting and obtaining a redshift for the lensing galaxy. This may be achievable with the *Hubble Space Telescope*.

We thank the referee for helpful comments which prompted refinements of the source model used in this work. This research was carried out at the Jet Propulsion Laboratory, California Institute of Technology, under contract with the National Aeronautics and Space Administration.

REFERENCES

Baars, J. W. M., Genzel, R., Pauliny-Toth, I. I. K., & Witzel, A. 1977, A&A, 61, 993
Djorgovski, S., et al. 1992, MNRAS, 257, 240
Jauncey, D. L., et al. 1993, in Sub-arcsecond Radio Astronomy, ed. R. J. Davis & R. S. Booth (Cambridge: Cambridge Univ. Press), 134
Jauncey, D. L., et al. 1991, Nature, 352, 132
King, E. A. 1994, Ph.D. thesis, Univ. Tasmania
Refsdal, S. 1964, MNRAS, 128, 295
Subrahmanyan, R., Narasimhar, D., Rao, A. P., & Swarup, G. 1990, MNRAS, 246, 263 (SNRS)
Nair, S., Narasimhar, D., & Rao, A. P. 1993, ApJ, 407, 46 (NNR)
Perley, R. A. 1994, Very Large Array Observational Status Summary (Socorro: NRAO)
Rao, A. P., & Subrahmanyan, R. 1988, MNRAS, 231, 229